ISSN 1063-7834, Physics of the Solid State, 2011, Vol. 53, No. 3, pp. 564–569. © Pleiades Publishing, Ltd., 2011.
Original Russian Text © K.S. Aleksandrov, N.V. Voronov, A.N. Vtyurin, A.S. Krylov, M.S. Molokeev, A.S. Oreshonkov, S.V. Goryainov, A.Yu. Likhacheva, A.I. Ancharov, 2011, published in Fizika Tverdogo Tela, 2011, Vol. 53, No. 3, pp. 527–531.

LATTICE DYNAMICS

Structure and Lattice Dynamics of the High-Pressure Phase in the ScF_3 Crystal

K. S. Aleksandrov[a,†], N. V. Voronov[a], A. N. Vtyurin[a,*], A. S. Krylov[a], M. S. Molokeev[a], A. S. Oreshonkov[a], S. V. Goryainov[b], A. Yu. Likhacheva[b], and A. I. Ancharov[c]

[a] *Kirensky Institute of Physics, Siberian Branch, Russian Academy of Sciences, Akademgorodok, Krasnoyarsk, 660036 Russia*
** e-mail: vtyurin@iph.krasn.ru*

[b] *Sobolev Institute of Geology and Mineralogy, Siberian Branch, Russian Academy of Sciences, pr. Akademika Koptyuga 3, Novosibirsk, 630090 Russia*

[c] *Institute of Solid State Chemistry and Mechanochemistry, Siberian Branch, Russian Academy of Sciences, ul. Kutateladze 18, Novosibirsk, 630128 Russia*

Received May 25, 2010

Abstract—The high-pressure phase of the ScF_3 crystal has been studied using synchrotron radiation diffraction and Raman scattering. This phase existing in the pressure range 0.6–3.2 GPa is optically anisotropic: its structure is described by space group $R\bar{3}c$, $Z = 2$, and the transition is associated with the rotation of ScF_6 octahedra around the threefold axis. The pressure dependences of the lattice parameters and the rotation angle have been determined. The number of lines in the Raman spectrum corresponds to the expected number for this structure; the recovery of soft modes has been observed above the phase transition.

DOI: 10.1134/S1063783411030036

1. INTRODUCTION

Trivalent metal fluorides MeF_3 with an ideal or distorted structure of α-ReO_3 belong to the family of perovskite-like compounds of the general formula ABX_3, in which one cation site is vacant (Fig. 1). Like all perovskites, these crystals undergo sequential phase transitions due to a change in ambient conditions (temperature and pressure). The simplicity of the structure makes them attractive as model objects for studying the mechanisms of phase transitions (see, for example, [1]), and the presence of bulky cavities in the structure makes it possible to flexibly change the physical properties of these crystals by doping or introducing a structural disorder, which has opened possibilities for developing practical applications based on these materials [2, 3].

Scandium fluoride is probably the least studied compound among the MeF_3 fluorides. There is no relevant information about this compound in the most comprehensive reviews on structural phase transitions in perovskites [4, 5]. The structural database [6] contains information about three different structures obtained on powder samples under normal conditions, namely, the cubic, rhombohedral, and orthorhombic structures. However, it was found that the orthorhombic phase under normal conditions is metastable [7]; at the same time, the cubic phase was not observed at all. According to the studies of the ScF_3 single crystal [8, 9], the cubic phase is stable under normal conditions; in contrast to a number of other perovskite-like trifluorides [5], it remains stable down

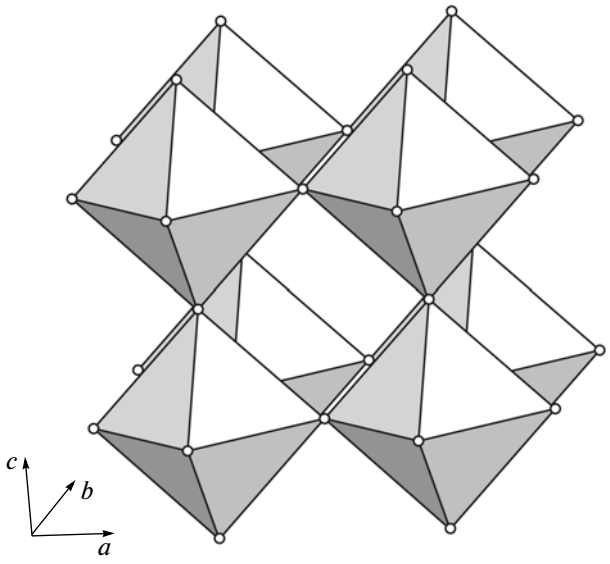

Fig. 1. Structure of the ScF_3 cubic phase. Shown are only the fluorine ions. The scandium ions are located at the centers of the ScF_6 octahedra.

† Deceased.

Table 1. Parameters of data acquisition and results of refinement of the ScF_3 structure in the high-pressure phase

Pressure P, GPa	Space group	a, Å	c, Å	V, Å^3	Range of angles 2θ, deg	Number of Bragg reflections	Number of refined parameters	B_{wp}, %	R_B, %
1.38	$R\bar{3}c/R3c$	5.3089(1)	14.0704(5)	343.43(2)	5–23	53	8/10	13.7/13.4	6.22/5.95
2.1	$R\bar{3}c/R3c$	5.2444(3)	14.1092(9)	336.07(4)	5–20	35	8/10	11.9/12.1	13.3/13.4
2.62	$R\bar{3}c/R3c$	5.0785(4)	14.277(1)	318.90(5)	5–23	51	8/10	17.2/16.7	9.96/9.76
3.25	$R\bar{3}c/R3c$	5.0449(1)	14.2605(5)	314.32(2)	5–20	33	8/10	8.29/8.27	6.78/6.40

to liquid-helium temperatures. Furthermore, under hydrostatic pressure, the ScF_3 single crystals undergo a phase transition to the rhombohedral phase [9]; however, the data on the space group and structure of this phase, which were obtained in our previous work [10], are contradictory. In this respect, the present work was aimed at studying the structure of the ScF_3 high-pressure phase and its lattice dynamics by X-ray diffraction and Raman scattering.

2. STRUCTURE OF THE HIGH-PRESSURE PHASE

The X-ray diffraction pattern of the polycrystalline ScF_3 sample was recorded at room temperature on a powder diffractometer with a MAR3450 area detector with the use of the $\lambda = 0.36750$ Å synchrotron radiation of the VEPP-3 accelerator at the Institute of Nuclear Physics (Siberian Branch, Russian Academy of Sciences, Novosibirsk).

The powdered ScF_3 samples under hydrostatic pressure at room temperature were studied on a setup with diamond anvils described in [11]. The diameter and height of the chamber with the sample were equal to 0.25 and 0.10 mm, respectively. The pressure was determined with an accuracy of 0.05 GPa from the shift of the luminescence band of a ruby microcrystal placed in the chamber. Ethanol–methanol mixtures or glycerin were used as pressure transmitting media.

The search for the centers of the rings and integration of the X-ray powder diffraction patterns were performed with the Fit2D program [12]; the X-ray powder diffraction patterns agree well with those presented in [10]. The lattice parameters determined with the WTREOR program [13] are listed in Table 1. Figure 2 shows the pressure dependence of the lattice parameters. The space groups of the compound at different pressures were found from the corresponding extinctions. It was found that, at all experimental pressures, the extinctions correspond to the space groups $R3c$ or $R\bar{3}c$. The search for structures was performed with the FOX program [14]. The values were further refined by the full-profile Rietveld method with the WINPLOTR program [15]. The main parameters of the data acquisition and structure refinement are listed in Table 1. The structure refinement in space groups $R3c$ and $R\bar{3}c$ was performed with the same experimental data. It was found that the profile and integral uncertainty factors slightly increase in some cases when changing over from the group $R3c$ [10] to the nonpolar group $R\bar{3}c$ but the number of refined parameters simultaneously decreases (Table 1) due to the displacement of the fluorine atom from the general position to the special position. The Hamiltonian criterion [16] allows one to compare the structure models with different numbers of refined parameters; the use of this crite-

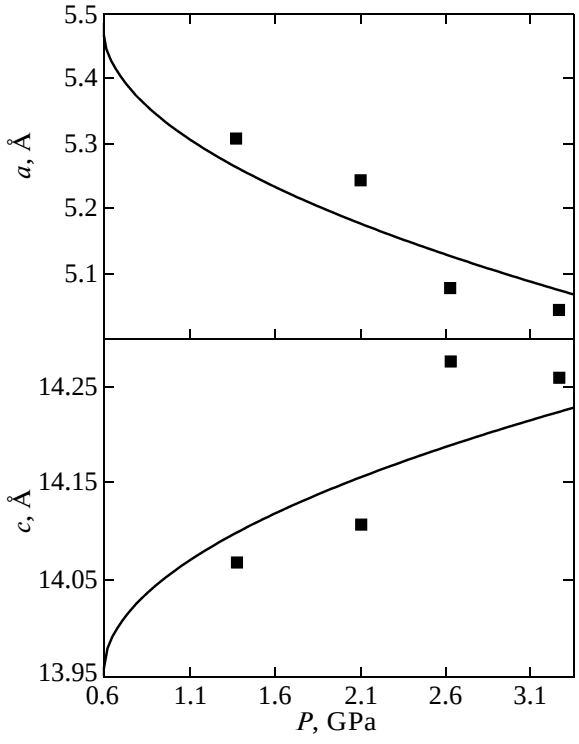

Fig. 2. Pressure dependences of the lattice parameters of the ScF_3 rhombohedral phase. The experimental data are interpolated by the curves $(P - P_0)^{1/2}$.

Table 2. Atomic coordinates and isotropic thermal parameters B_{iso} in ScF_3 at different pressures

Atom	Site occupancy	x	y	z	B_{iso}, Å^2
$P = 1.38$ GPa					
Sc	1.0	0	0	0	1.32(9)
F	1.0	0.60125(3)	0.60125(3)	0.25	1.03(9)
$P = 2.10$ GPa					
Sc	1.0	0	0	0	1.80(9)
F	1.0	0.6023(6)	0.6023(6)	0.25	0.6(1)
$P = 2.62$ GPa					
Sc	1.0	0	0	0	0.24(6)
F	1.0	0.6336(7)	0.6336(7)	0.25	0.1(1)
$P = 3.25$ GPa					
Sc	1.0	0	0	0	1.16(5)
F	1.0	0.6309(4)	0.6309(4)	0.25	0.59(7)

rion leads to a 99.5% probability for the model with the centrosymmetric group $R\bar{3}c$.

The peak shapes were described using the Pearson VII function with an FWHM of 6.0 in order to refine the profile and with an FWHM of 20.0 for the final refinement of the structure, where FWHM is the full width at half-maximum. All stages of the refinement were similar to those described in our previous work [10]. The results of the structure refinement are presented in Table 2.

According to the structure analysis of the high-pressure phase, the ScF_6 octahedron rotates around the threefold axis upon the phase transition; in this case, all eight Sc–F bond lengths remain equal and the center of the ScF_6 group coincides with the inversion center. The length of the Sc—F bonds varies within the range 1.97–2.00 Å under different pressures, which is much narrower than the range 1.9–2.1 Å obtained in our previous work [10] from the structure refinement for group $R3c$ and close to the Sc–F bond length under normal conditions (2.01 Å).

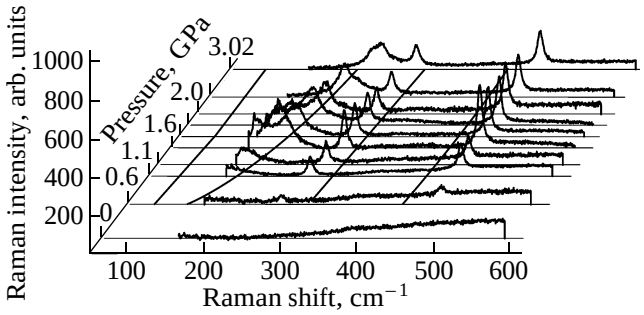

Fig. 3. Transformation of the Raman spectrum with an increase in the pressure. Curves in the horizontal plane represent the frequencies obtained from the model calculation.

3. VARIATIONS OF THE RAMAN SPECTRA

The vibrational representation of space group $Pm\bar{3}m$ of the cubic phase for the center of the Brillouin zone has the form

$$\Gamma_0 = F_{2u} + 3F_{1u}. \quad (1)$$

In this case, all vibrations are Raman-inactive modes.

Similar expansions for the rhombohedral structures $R\bar{3}c$ and $R3c$ have the form

$$\Gamma_{R\bar{3}c} = \mathbf{A_{1g}} + 2A_{2g} + 3\mathbf{E_g} + 2A_{1u} + 3A_{2u} + 5E_u \quad (2)$$

and

$$\Gamma_{R3c} = 4\mathbf{A}_1 + 4A_2 + 8\mathbf{E}, \quad (3)$$

respectively. In Eqs. (2) and (3), the Raman-active modes are typed in bold. As follows from comparison of Eqs. (1)–(3), the selection rules for these structures differ significantly, and the structures should be easily identified using the Raman spectra.

The Raman spectra of unoriented single crystals were excited by the radiation from an Ar^+ laser (514.5 nm, 0.2 W) and recorded on a Horiba–Jobin–Yvon T-64000 multichannel spectrometer. High hydrostatic pressure was produced and measured using the same technique and equipment as in the X-ray structural investigations. Because of the small size of the samples and strong diffuse scattering, only the high-frequency (150–600 cm^{-1}) part of the spectrum was recorded. The domain structure and the effects of birefringence in the sample were simultaneously observed with a polarizing microscope.

Table 3. Parameters of the interatomic interaction potential

Bond	λ, 10^{-18} J	ρ, Å	z_F
$P = 1.38$ GPa			
Sc–F	1630	0.20031	–0.7
F–F	151	0.283	–0.7
$P = 2.10$ GPa			
Sc–F	1640	0.199	–0.7
F–F	178	0.281	–0.7
$P = 2.65$ GPa			
Sc–F	1623	0.20063	–0.7
F–F	185	0.283	–0.7
$P = 3.25$ GPa			
Sc–F	1637	0.199	–0.7
F–F	211	0.281(4)	–0.7

At normal pressure, Raman scattering in the crystal sample is absent; the crystal is optically isotropic and exhibits good extinction between crossed polarizers (slight bleaching is observed under pressure due to anisotropic mechanical stresses in the diamond anvils). At a pressure of 0.6 GPa, the spectrum exhibits two weak lines at 263 and 473 cm^{-1} (Fig. 3); simultaneously, there occurs a bleaching of the sample placed between the crossed polarizers, which indicates the appearance of optical anisotropy. In some samples, separation into coarse (about 0.02–0.05 mm) irregular-shaped domains takes place. As the pressure increases further, the intensity of the observed lines increases monotonically, and the low-frequency line shifts from 263 to 303 cm^{-1} at 3.0 GPa. In the low-frequency range, a line at 144 cm^{-1} appears at 1.1 GPa, which monotonically shifts to 243 cm^{-1} at 3.0 GPa. Note that the excitation radiation is newly focused after each pressure change, thus making correct measurement of the line intensity ratio impossible.

4. RESULTS AND DISCUSSION

In our previous work [10], the vibrational spectrum of the ScF_3 lattice and the effect of pressure on the crystal structure were calculated with the use of the ab initio model of an ionic crystal, which generalizes the Gordon–Kim approximation taking into account the effect of the crystal lattice on the deformability and polarizability of ions. However, the calculation yielded somewhat underestimated values of frequencies as compared to the experiment.

In this work, interionic interactions were calculated with the use of empirical potentials implemented in the LADY program package [17]. Different potential models were analyzed by means of this package; it turned out that already quite simple and common model of rigid ions is appropriate for describing the crystal under consideration.

This model describes the interaction of isolated spherical ions with charge z_i. The potential function is expressed as the sum of the Coulomb and short-range interionic interaction potentials

$$V^{\mathrm{RIM}}(r_{ij}) = \frac{1}{2}\sum_{i,j}\frac{z_i z_j}{r_{ij}} + U(r_{ij}). \quad (4)$$

The short-range interaction potential was taken in the Born–Mayer form

$$U(r_{ij}) = \lambda e^{(-r_{ij}/\rho)}, \quad (5)$$

where r_{ij} is the interatomic distance and λ and ρ are the parameters of the short-range pair interionic interaction. In the calculations, it is convenient to change over from the parameters λ and ρ to the parameters A and B defined as

$$A = \frac{\partial^2 U}{\partial r^2}, \quad B = \frac{1}{r}\frac{\partial U}{\partial r}, \quad (6)$$

from where we obtain

$$\frac{A}{B} = -\frac{r}{\rho}. \quad (7)$$

It was previously found [18] that the ratio A/B and charge z_F of the fluorine ion in trifluorides MeF_3 (Me = Al, Cr, Ga, V, Fe, In) isomorphic to ScF_3 ranges from –9.5 to –11.5 and from –0.644 to –0.701 (in units of electron charge), respectively. The parameters

Table 4. Frequencies of Raman-active vibrations of the ScF_3 rhombohedral phase (cm^{-1})

Pressure P, GPa	Symmetry of vibrations			
	A_{1g}	E_g	E_g	E_g
1.38	173 (170)	100	289 (289)	420 (460)
2.10	176 (230)	97.3 (160)	299 (290)	425 (456)
2.62	222.1 (240)	113.4	300.2 (300)	413 (450)
3.25	222.3 (260)	109.5	309.2 (305)	418.1 (455)

Note: Experimental values are given in parentheses.

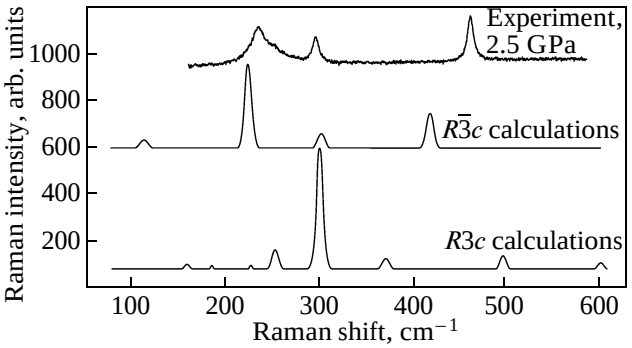

Fig. 4. Comparison of the calculated Raman spectra of the $R3c$ and $R\bar{3}c$ phases with the experimental spectrum.

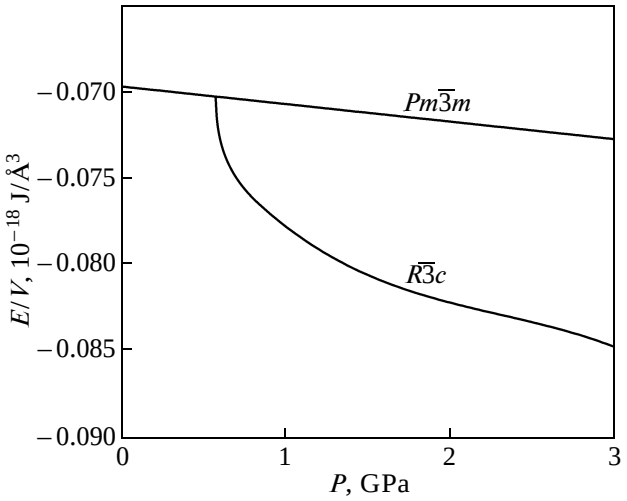

Fig. 5. Pressure dependences of the energy density of the cubic ($Pm\bar{3}m$) and rhombohedral ($R\bar{3}c$) lattices of ScF_3.

of the model were found with the use of these data as the initial experimental Raman spectra at 2.1 GPa and the structural parameters extrapolated to the same pressure taking into account the lattice stability at normal and increased hydrostatic pressures. The values of λ, ρ, and z_F obtained in such a manner for the ScF_3 crystal are listed in Table 3.

The spectra of the crystal under investigation at different pressures were calculated with the LADY program package. The resultant pressure dependence of the frequencies of Raman-active lines is shown in Fig. 3. The corresponding numerical values are given in Table 4. Clearly, there is good agreement of the calculated values with the experimental data.

Similar calculations were carried out for the high-pressure phase $R3c$ for comparison. Experimental and calculated spectra for the $R\bar{3}c$ and $R3c$ phases are compared in Fig. 4. As is seen, the number and position of the spectral lines in the latter case even qualitatively disagree with the experiment.

The vibrational spectrum of the ScF_3 lattice in the cubic phase under normal pressure, calculated at the same interaction parameters, does not include imaginary frequencies, which explains the structure stability. However, there is a weakly dispersion low-lying (between the points R and M of the Brillouin zone) branch of the spectrum. This triply degenerate mode R_5 corresponds to displacements of fluorine ions due to rotations of the ScF_6 octahedra around the threefold axes of the cubic structure. A decrease in the parameter of the cubic unit cell, which corresponds to an increase in the pressure, leads to a decrease in the frequency of this dispersion branch.

The energy density of the ScF_3 crystal as a function of pressure was calculated for the cubic and rhombohedral $R\bar{3}c$ structures with the use of the found parameters of the potential; the calculation results are shown in Fig. 5. The found dependences indicate that the rhombohedral structure $R\bar{3}c$ becomes energetically more favorable for ScF_3 above 0.6 GPa. Note that neither the frequency of the above-mentioned dispersion branch R_5 nor the frequencies of low-lying vibrations A_{1g} and E_g vanish (although they decrease substantially when this pressure is approached); consequently, this point corresponds to the first-order phase transition.

5. CONCLUSIONS

Thus, the structure of the ScF_3 crystal under hydrostatic pressure has been refined and its lattice dynamics has been numerically calculated.

According to the X-ray structure analysis and Raman spectroscopy, the structure of the phase experimentally revealed above 0.6 GPa is described by space group $R\bar{3}c$. The transition induced by hydrostatic pressure occurs due to imbalance of the long-range Coulomb and short-range interactions of ions and is associated with rotation of ScF_6 octahedra around the threefold axis. Calculations within the empirical model indicate that the observed transition point corresponds to the first-order phase transition.

ACKNOWLEDGMENTS

This study was supported by the Siberian Branch of the Russian Academy of Sciences within the framework of the integration project no. 3.7

REFERENCES

1. Ph. Daniel, A. Bulou, M. Rousseau, J. L. Fourquet, M. Leblanc, and R. Burriel, J. Phys.: Condens. Matter **2**, 5663 (1990).
2. K. Rotereau, Ph. Daniel, and J. Y. Gesland, J. Phys. Chem. Solids **59**, 969 (1998).
3. K. Rotereau, Ph. Daniel, A. Desert, and J. Y. Gesland, J. Phys.: Condens. Matter **10**, 1431 (1998).
4. K. S. Aleksandrov, A. T. Anistratov, B. V. Beznosikov, and N. V. Fedoseeva, *Phase Transitions in ABX_3 Crystals* (Nauka, Novosibirsk, 1981) [in Russian].
5. D. Babel and A. Tressaud, in *Inorganic Solid Fluorides* (Academic, London, 1985), p. 77.
6. *Powder Diffraction Data, Nos. 75-0877, 46-1243, 44-1096, 43-1145, 32-0989, and 17-0836* (International Center for Diffraction Data, Newtown Square, Pennsylvania, United States, 1999).
7. M. M. Aleksandrova, N. A. Bendeliani, V. D. Blank, and T. I. Dyuzheva, Izv. Akad. Nauk SSSR, Neorg. Mater. **26**, 1028 (1990).
8. V. I. Zinenko and N. G. Zamkova, Fiz. Tverd. Tela (St. Petersburg) **42** (7), 1310 (2000) [Phys. Solid State **42** (7), 1348 (2000)].
9. K. S. Aleksandrov, V. N. Voronov, A. N. Vtyurin, S. V. Goryainov, N. G. Zamkova, V. I. Zinenko, and A. S. Krylov, Zh. Eksp. Teor. Fiz. **121** (5), 1139 (2002) [JETP **94** (5), 977 (2002)].
10. K. S. Aleksandrov, V. N. Voronov, A. N. Vtyurin, A. S. Krylov, M. S. Molokeev, M. S. Pavlovskii, S. V. Goryainov, A. Yu. Likhacheva, and A. I. Ancharov, Fiz. Tverd. Tela (St. Petersburg) **51** (4), 764 (2009) [Phys. Solid State **51** (4), 810 (2009)].
11. S. V. Goryainov and I. A. Belitsky, Phys. Chem. Miner. **22**, 443 (1995).
12. A. P. Hammersley, *FIT2D: An Introduction and Overview* (European Synchrotron Radiation Facility (ESRF) Internal Report, No. ESRF97HA02T, Grenoble, France, 1997).
13. P.-E. Werner, L. Eriksson, and M. Westdahl, J. Appl. Crystallogr. **18**, 367 (1985).
14. V. Favre-Nicolin and R. Černý, J. Appl. Crystallogr. **35**, 734 (2002).
15. T. Roisnel and J. Rodríquez-Carvajal, Mater. Sci. Forum **378–381**, 118 (2001).
16. W. C. Hammilton, Acta Crystallogr. **18**, 502 (1965).
17. M. B. Smirnov and V. Yu. Kazimirov, *LADY: Software for Lattice Dynamics Simulations* (JINR Commun., No. E14-2001-159 (2001)).
18. P. Daniel, A. Bulou, M. Rousseau, J. Nouet, and M. Leblanc, Phys. Rev. B: Condens. Matter **42**, 10545 (1990).

Translated by A. Safonov